Acta Geophysica (2024) 72:3595–3607
https://doi.org/10.1007/s11600-023-01273-4

SHORT COMMUNICATION - HYDROLOGY AND HYDRAULICS

A new method for preventing sidewall preferential flow in the internal erosion simulation using un-resolved CFD–DEM

Leilei Liu[1,2] · Rui Chen[1,2] · Zhaofeng Li[1] · Chao Zhou[1,3] · Xiaojiao Li[1]

Received: 7 August 2023 / Accepted: 6 December 2023 / Published online: 23 January 2024

Abstract

Accurately assessing the erodibility of geomaterials is of great significance for the design of earthen structures and the prevention of the associated failure induced by seepage force. Recently, the un-resolved Computational Fluid Dynamics–Discrete Element Method (CFD–DEM) has been widely used to investigate internal erosion. However, due to the use of wall boundary and the fact that the fixed CFD domain cannot be changed with the soil sample's volume contraction during the erosion test, a larger porosity at the boundary of the CFD domain is commonly formed, resulting in sidewall preferential flow (i.e., relatively more fine particles migrate along the boundary of the DEM domain) and thereby overestimating the soil erodibility. In this study, a new method based on particle boundary is developed to tackle this problem. The newly proposed particle boundary can prevent its particles from erosion via inter-particle bonding and transfer stress from servo walls to the simulated sample. An optimal particle boundary thickness is determined by considering sample contraction and computational efficiency. The performance of the new method was compared with the conventional method and also verified using experimental results. The results show that the newly proposed method has significantly improved the uniformity of fluid velocity distribution. Furthermore, the cumulative eroded mass of fine particles in the new model is approximately 15% lower than in the conventional model. It is convincingly demonstrated that the new method can simulate internal erosion better and give a more accurate assessment of geomaterial erodibility.

Keywords Seepage · Internal erosion · CFD–DEM · Modeling method

Introduction

Soil erosion generally includes internal erosion and surface erosion. Seepage-induced internal erosion would lead to a change in soil properties (e.g., porosity, permeability, and shear strength) (Bora et al. 2022; Garg et al. 2022; Li et al. 2023), which ultimately lead to the failures of hydraulic geo-structures such as earth dams, embankments and dikes (ICOLD 2013). Numerous experimental and numerical studies have been carried out to investigate the macroscopic and microscopic behavior of internal erosion (Bendahmane et al. 2008; Chen et al. 2021; Cheng et al. 2021; Ke and Takahashi 2014; Li and Li 2023; Nie et al. 2023; Zhao and Shan 2013). In addition, there have been recent developments in theoretical models utilizing erosion constitutive laws for simulating internal erosion (e.g., Bora et al. 2023; Cai et al. 2023). It is worth noting that, the unresolved CFD–DEM approach has recently received much attention because of its relatively higher computational efficiency than the fully-resolved or semi-resolved CFD–DEM (Cheng et al. 2021; Nijssen et al. 2023). It can reveal the evolution of soil microstructure during erosion (Liu et al. 2023; Mu et al. 2022).

In existing unresolved CFD–DEM simulations, a representative volume element (RVE) is generally modeled using 5000 to 50,000 particles and 5 to 10 fluid cells in each direction of the model. Rigid and planar walls are commonly generated to serve as boundaries of the RVE, such as the

Edited by Dr. Ankit Garg (ASSOCIATE EDITOR) / Prof. Jochen Aberle (CO-EDITOR-IN-CHIEF).

✉ Chao Zhou
c.zhou@polyu.edu.hk

[1] School of Civil and Environmental Engineering, Harbin Institute of Technology, Shenzhen, Shenzhen 518055, China

[2] Guangdong Provincial Key Laboratory of Intelligent and Resilient Structures for Civil Engineering, Shenzhen 518055, China

[3] Department of Civil and Environmental Engineering, The Hong Kong Polytechnic University, Hung Hom, Hong Kong, China

modeling in Hu et al. (2019, 2020), Wang et al. (2022), and Zhang et al. (2023). As a result of using these wall boundaries, sidewall preferential flow typically occurs during seepage testing (Kim et al. 2019; Premkumar et al. 2016). For instance, in the studies by Hu et al. (2019, 2020), it was observed that due to the preferential flow near the perimeter of the sample, most fine particles adjacent to the wall are eroded, while the center of the sample does not have obvious erosion. It is worth noting that many researchers have recognized the issue of sidewall preferential flow, especially in laboratory experiments, and several methods have been proposed to prevent this problem, as it often determines the success or failure of experiments. For example, Chen et al. (2021) used Vaseline to coat the sidewalls of the permeameter in suffusion tests, and Zhou et al. (2018) applied latex membranes inside the test chamber to prevent sidewall preferential flow, yielding favorable experimental outcomes. These findings emphasize the significance of preventing sidewall preferential flow. However, there have been limited numerical simulation studies addressing this problem, which might lead to an overestimation of soil erosion development, subsequently impacting the accurate assessment of the erodibility of geomaterials.

Figure 1 shows the cross-section of a cubic soil sample perpendicular to the seepage direction using the conventional modeling method. Pore W near the wall is larger than pore P inside the sample, leading to a higher fluid velocity near the boundary. The fluid cells in the CFD domain are fixed, and their range is generally identical to the initial sample size defined in the DEM domain. Figure 2 illustrates the distribution of fluid cells under two different boundary conditions: (i) non-displacement boundary; and (ii)

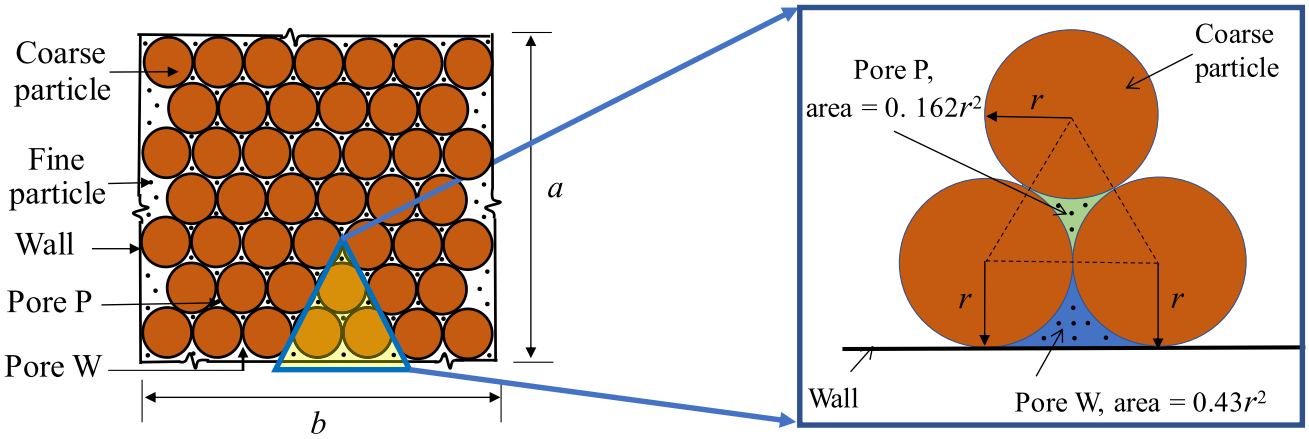

Fig. 1 Schematic diagram of the conventional method: a cross-section of soil sample perpendicular to seepage direction

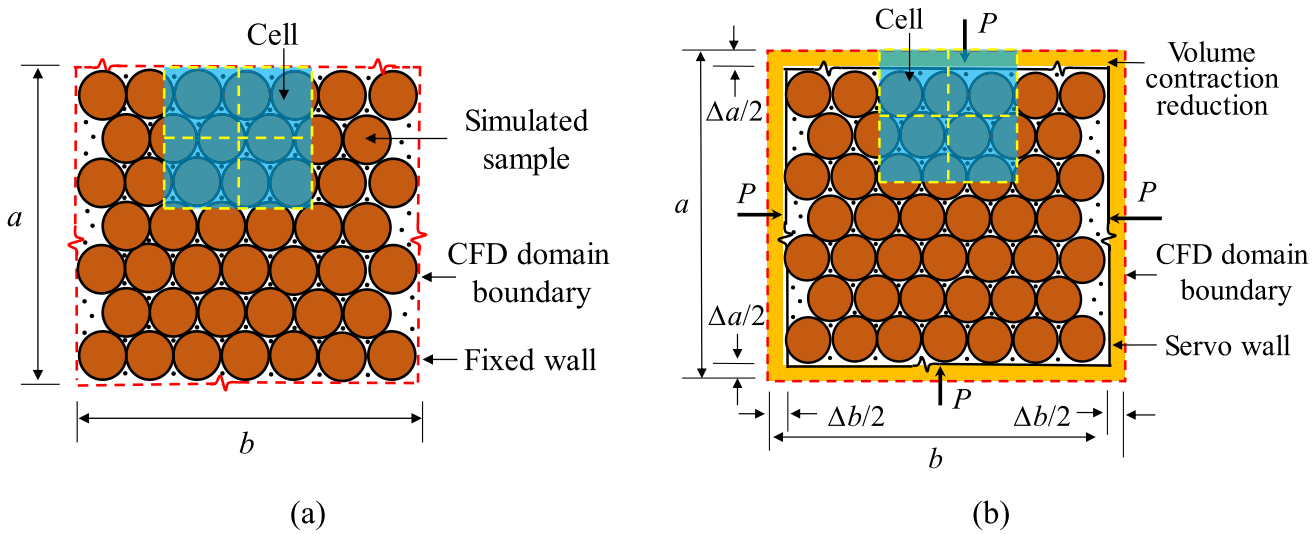

Fig. 2 Fluid cells in the conventional method under different boundary conditions: **a** non-displacement boundary; **b** constant-stress boundary using a servo-controlled approach

constant-stress boundary using a servo-controlled approach. In the latter case, the sample in the DEM domain may experience significant volumetric contraction during consolidation and erosion. Therefore, the CFD domain becomes larger than the DEM domain. The porosity of fluid cells and the predicted water velocity at the boundary of the DEM domain would become very large. Given the above two problems, the water flow velocity is higher near the wall boundary, inducing the sidewall preferential flow (Hu et al. 2020). Consequently, more fine particles migrate along the wall boundary (Nguyen and Indraratna 2020; Xiong et al. 2021; Zou et al. 2020), overestimating the erosion initiation and development (i.e., soil erodibility).

Some recent studies have attempted to tackle this problem. Gu et al. (2019) created a much larger granular assembly (i.e., DEM domain). Other particles surrounding the numerical sample were treated as particle boundaries, and their locations were fixed. Liu et al. (2020) built a granular assembly slightly larger than the sample, but they did not propose a method to determine the size of the DEM domain. The above approaches only overcome wall boundary deficiency and are suitable for erosion tests involving little or no sample volume change. However, preferential flow still occurs if the sample volume decreases significantly during the erosion stage. Therefore, a more efficient method for preventing preferential flow is desired. It is worth noting that periodic boundary conditions can help reduce the high porosity caused by the rigid and planar walls. However, for a sample with a given volume, it may lead to additional fines loss due to volumetric contraction at the periodic boundary. This might explain why the existing CFD–DEM studies have not utilized this approach (e.g., Gu et al. 2019; Shi et al. 2018; Zou et al. 2020).

In this study, a new un-resolved CFD–DEM modeling method is developed to simulate internal erosion without sidewall preferential flow. In the following sections, the modeling methods are first introduced. Then, numerical simulations are conducted to compare the efficiency of the new and conventional modeling approaches. Finally, the performance of the new method is justified by a one-way analysis of variance (ANOVA) and verified using experimental data from the literature.

A new modeling method for coupled CFD–DEM

As explained above, the use of wall boundaries is a major reason for the preferential flow. To address this problem, particle boundary is used for the numerical sample based on the principle of flexible membrane boundary (Cheung and O'Sullivan 2008). In other words, coarse particles are added around the numerical sample (see Fig. 3), where both micro and macro behaviors of soil particles are determined and analyzed. These added particles are treated as a particle boundary of the numerical sample to reduce pore size near the walls. Moreover, a linear contact bond model (Itasca Consulting Group, 2015) is set at the inter-particle contacts

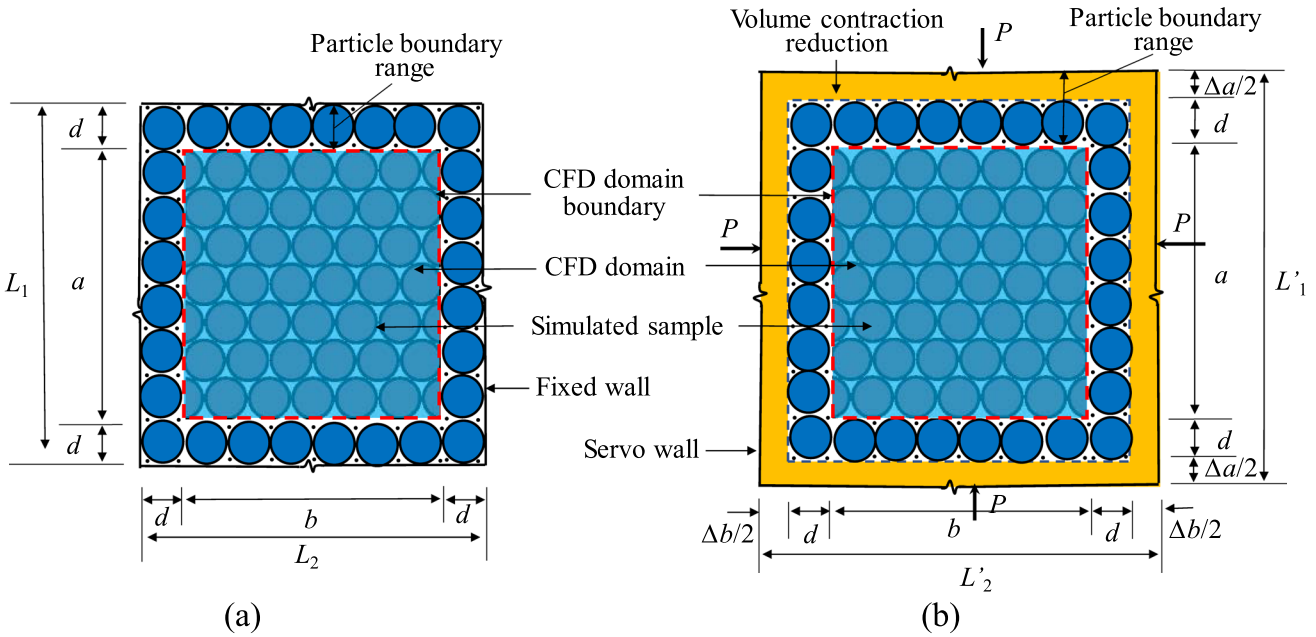

Fig. 3 Schematic diagram of the new modeling method under different boundary conditions: **a** non-displacement boundary; **b** constant-stress boundary using a servo-controlled approach

inside the particle boundary, so that these newly-added particles are not dragged away by seepage force (Li et al. 2017).

On the other hand, the preferential flow is intensified by volumetric contraction, which leads to a gap between the CFD domain boundary and the sample boundary (see Fig. 2b). From the perspective of eliminating preferential flow, a thicker particle boundary is preferred. In fact, if numerical computational efficiency is not the primary concern, the thickness of the particle boundary can be quite substantial. However, the thickness of the particle boundary should not be too large because the CFD–DEM coupled analysis is very time-consuming. Therefore, an optimal thickness of the particle boundary needs to be determined to seek good computational efficiency and accuracy. Considering that the CFD and DEM programs run separately when not coupled, DEM's computational domain can be set larger than CFD's. For a given numerical sample (a in height and b in width, equal to the size of the CFD domain), the initial size of the DEM domain is determined as follows:

Under non-displacement conditions (see Fig. 3a), only one row/column of coarse particles is used along each side, sufficient to reduce the porosity near the boundary walls. Therefore, the new model's dimensions can be determined by Eqs. (1 and 2):

$$L_1 = a + 2d, \tag{1}$$

$$L_2 = b + 2d, \tag{2}$$

where L_1 and L_2 are the height and width of the new model under non-displacement conditions, respectively; d is the average diameter of coarse particles.

For the sample under constant-stress conditions (see Fig. 3b), it is necessary to consider the volume contraction (i.e., radial or axial strain) in addition to the above consideration. By modifying Eqs. (1 and 2), the size of the DEM domain is as follows:

$$L_1' = a + 2d + \Delta a, \tag{3}$$

$$L_2' = b + 2d + \Delta b, \tag{4}$$

where L'_1 and L'_2 are the height and width of the new model under constant-stress conditions, respectively; Δa and Δb denote the reductions in height and width of the original model due to consolidation and seepage erosion, respectively, which can be determined by some preliminary tests.

It should be noted that the size of the above new model is relatively optimal for ensuring good computation efficiency and accuracy. The dimension in the third direction can also be determined similarly. Given that fine particles occupy the inter-particle voids among the coarse particles, their impact on the thickness of the particle boundary is negligible. Therefore, when determining the thickness of the particle boundary, we consider only the presence of coarse particles. The particle boundary and the numerical sample are simultaneously generated as they are set to be the same particle size distribution (PSD). This means that the particle boundary includes a mixture of coarse and fine particles. To prevent the finer particles in the boundary from being dragged away by seepage force, a bonding is set at the inter-particle contacts inside the particle boundary.

Performance of the new modeling method

Coupled CFD–DEM method

Numerical simulations were carried out to evaluate the new method's performance. All simulations are implemented in the PFC3D program using a fixed coarse mesh scheme (i.e., a so-called un-resolved method) (Yao et al. 2020). The methodology details on the coupled CFD-DEM are briefly introduced below.

Governing equations for fluid phase

In the CFD domain, the fluid flow is governed by the continuity and locally averaged Navier-Stokes equations (Hu et al. 2020; Nguyen and Indraratna 2020), as shown in Eqs. (5 and 6):

$$\frac{\partial n}{\partial t} = -(\nabla \cdot n\boldsymbol{v}), \tag{5}$$

$$\frac{\partial (n\boldsymbol{v})}{\partial t} = -(\nabla \cdot n\boldsymbol{v}\boldsymbol{v}) - \frac{n}{\rho_{\mathrm{f}}}\nabla p - \frac{n}{\rho_{\mathrm{f}}}\nabla \cdot \boldsymbol{\tau} + n\boldsymbol{g} + \frac{\boldsymbol{f}_{\mathrm{int}}}{\rho_{\mathrm{f}}}, \tag{6}$$

where n is the porosity of a fluid cell; t is the time; $\boldsymbol{v}$ is the fluid velocity vector; ρ_f is the fluid density; p is the fluid pressure; ∇p is the gradient of fluid pressure; $\boldsymbol{\tau}$ is the viscous stress tensor; $\boldsymbol{g}$ is the gravity acceleration; $\boldsymbol{f}_{\mathrm{int}}$ is the interaction force per unit volume between the particles and fluid.

Governing equations for solid phase

In the DEM domain, the motions of solid particles are computed by Newton's second law of motion (Cundall and Strack 1979). The translational and rotational motions of particles are governed by the following equations:

$$\frac{\partial \boldsymbol{u}}{\partial t} = \frac{\boldsymbol{f}_{\mathrm{mech}} + \boldsymbol{f}_{\mathrm{fluid}}}{m} + \boldsymbol{g}, \tag{7}$$

$$\frac{\partial \boldsymbol{w}}{\partial t} = \frac{\boldsymbol{M}}{I}, \tag{8}$$

where $\boldsymbol{u}$ is the particle velocity vector; m is the particle mass; $\boldsymbol{f}_{\text{mech}}$ is the sum of additional forces acting on the particle; $\boldsymbol{f}_{\text{fluid}}$ is the total force (the drag force and the pressure gradient force) applied by the fluid on the particle; $\boldsymbol{w}$ is the particle angular velocity; I is the moment of inertia, and $\boldsymbol{M}$ is the moment acting on the particle.

Fluid–solid interaction

In this study, the predominant forces between the particle and fluid, including the drag force $\boldsymbol{f}_{\text{d}}$ and the pressure gradient force $\boldsymbol{f}_{\nabla \text{p}}$ are considered (Wang et al. 2022). The total fluid-particle interaction force on an individual particle can be written as:

$$\boldsymbol{f}_{\text{fluid}} = \boldsymbol{f}_{\text{d}} + \boldsymbol{f}_{\nabla \text{p}}. \tag{9}$$

The pressure gradient force $\boldsymbol{f}_{\nabla \text{p}}$ is calculated according to the expression:

$$\boldsymbol{f}_{\nabla \text{p}} = V_p \nabla p, \tag{10}$$

where the V_p is the volume of the particle, the drag force can be expressed by the theory of Di Felice (1994):

$$\begin{cases} \boldsymbol{f}_{\text{d}} = \dfrac{1}{8} C_d \rho_f \pi d_p^2 (\boldsymbol{u} - \boldsymbol{v}) |\boldsymbol{u} - \boldsymbol{v}| n^{-\chi} \\ C_d = \left(0.63 + \dfrac{4.8}{\sqrt{Re_p}} \right)^2 \\ Re_p = \dfrac{\rho_f d_p |\boldsymbol{u} - \boldsymbol{v}|}{\mu_f} \\ \chi = 3.7 - 0.65 \exp\left[-\dfrac{(1.5 - \log_{10} Re_p)^2}{2} \right], \end{cases} \tag{11}$$

where d_p is the diameter of the particle; C_d is the particle–fluid drag coefficient depending on particle Reynolds number Re_p; μ_f is the dynamic viscosity; χ is the empirical coefficient to account for the local porosity.

Model implementation

Model setup

A cubic soil sample (14 mm × 14 mm × 14 mm) is simulated under isotropic stress of 50 kPa (e.g., Hu et al. 2019; Liu et al. 2020). The simulated sample here is a gap-graded mixture composed of fine particles with a radius of 0.25 mm and coarse particles with a radius of 1.0 mm, identical to Liu et al. (2020). According to the criterion proposed by Kézdi (1979), the simulated soil is internally unstable for internal erosion.

Based on some preliminary tests conducted on samples with fines contents of 15%, 25%, and 35% without considering sidewall preferential flow, it is observed that the maximum deformation (Δa or Δb) in each direction is around 0.5 mm during consolidation, and it is only about 0.02 mm during erosion, i.e.,, Δa or $\Delta b = 0.52$ mm. According to Eqs. (3 and 4) proposed in Sect. "A new modeling method for coupled CFD–DEM", $L'_1 = a + 2d + \Delta a = 18.52$ mm, and $L'_2 = b + 2d + \Delta b = 18.52$ mm, which is approximately 18.5 mm. Hence, the new model size is 18.5 mm × 18.5 mm × 18.5 mm (see Fig. 4b). Other configuration parameters are detailed in Table 1.

Numerical program

This study uses new and conventional methods to simulate erosion tests with different fines contents (FC). To further evaluate the model capability, numerical results from the new and the conventional methods were compared with experimental results in Ke and Takahashi (2014), which studied the seepage-induced erosion of a silica sand binary mixture. Three fine contents (i.e., FC = 15%, 25%, and 35%) were considered. It is worth noting that the experimental results are obtained using a triaxial permeameter using a flexible membrane, in which preferential flow can be effectively prevented. Details of the numerical program are summarized in Table 2.

Simulation procedure

The simulation procedure comprises four stages: sample generation, consolidation, reconsolidation, and erosion test. In the first stage, the granular assembly with the designated PSD is generated by randomly inserting sample particles in the three-dimensional(3D) cuboid domain (see Fig. 4). During the consolidation phase, the sample is isotropically confined to achieve the desired mean effective stress of 50 kPa. In the reconsolidation stage, the top wall is first replaced by a permeable wall (i.e., filter screen). Note that the filter has a mesh spacing 2.5 times larger than the average particle size of the fine particles, allowing fine particles to pass through. Besides, an inter-particle contact bonding (see Table 1) is set in the particle boundary to make them like a flexible membrane (Cheung and O'Sullivan 2008). Then, the isotropic stress of 50 kPa is again applied to the granular assembly. In the final stage, a relatively large hydraulic gradient, $i = 2.0$, and erosion time, $t = 15$ s, are selected for the erosion tests (Liu et al. 2020). Note that the 15 s duration is sufficient to allow erosion within the soil sample to reach its maximum extent, meaning that in the later stages of the test, no further fine particles are being eroded.

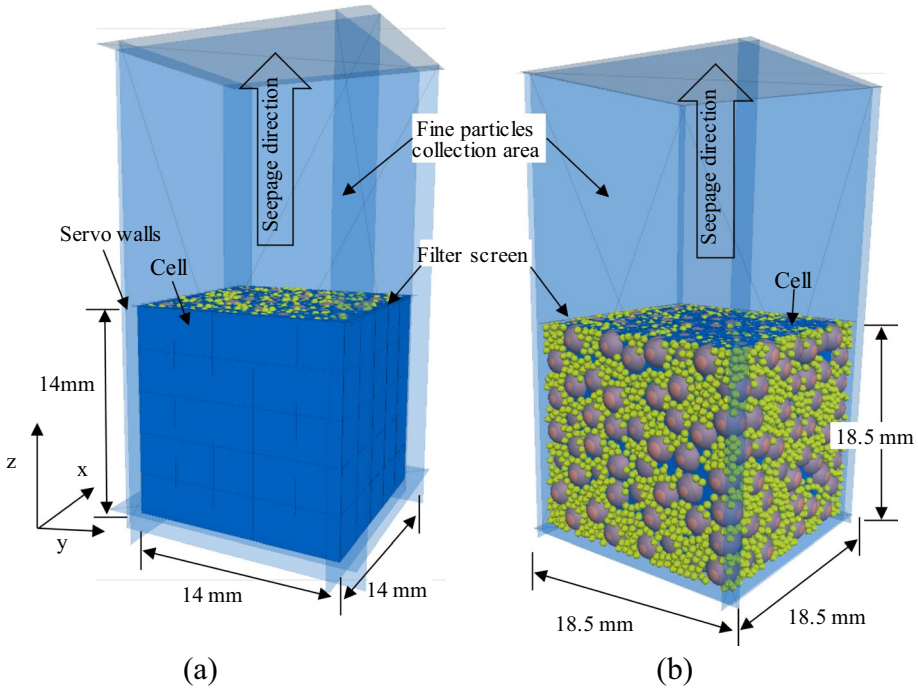

Fig. 4 Numerical models established by: **a** conventional method; **b** new method

Table 1 Summary of the numerical model parameters

Property names	Parameter types (units)	Values
Particle boundary	Particle Young's modulus (kPa)	3×10^4
	Normal and Shear bond strength (kPa)	4×10^3
	friction coefficient	0.0
Simulated sample	sample $L\times W\times H$ (mm)	$14\times14\times14$
Model dimension	New model $L\times W\times H$ (mm)	$18.5\times18.5\times18.5$
	Conventional model $L\times W\times H$ (mm)	$14\times14\times14$
Particle	Particle diameter (mm)	0.5 ~ 2.0
	Young's modulus (kPa)	3×10^4
	Poisson's ratio	0.3
	friction coefficient	0.3
Wall	Wall stiffness (N/m)	1×10^7
	friction coefficient	0.0
Fluid	Cell size (m^3)	$2.8\times2.8\times2.8$
	Density (Kg/m^3)	1×10^3
	Dynamic viscosity (Pa·s)	0.001
Coupling parameters	DEM timestep (s)	5×10^{-7}
	CFD timestep (s)	5×10^{-5}
	Coupling interval (s)	5×10^{-5}
	Simulation time (s)	15

Comparison between the new and conventional modeling methods

Comparison of fines loss

The cumulative eroded fines mass m_e, defined as the ratio of eroded fine particle mass to the initial total mass of the sample, is a crucial indicator of soil erosion degree. Figure 5 illustrates the evolution of m_e over time under varying fines content using the conventional and new modeling methods. It is evident that, for a given fines content, the m_e obtained using the new modeling method is consistently higher than that obtained using the conventional modeling method. For instance, in the case of FC15-Con, the m_e is 17% higher

Table 2 Simulation program

Case number	Model types	Hydraulic gradient, i	Isotropic stress, P (kPa)	Fines content, FC (%)	void ratio, e
FC15-New	New model	2.0	50	15	0.56
FC15-Con	Conventional model	2.0	50	15	0.56
FC25-New	New model	2.0	50	25	0.47
FC25-Con	Conventional model	2.0	50	25	0.47
FC35-New	New model	2.0	50	35	0.44
FC35-Con	Conventional model	2.0	50	35	0.44

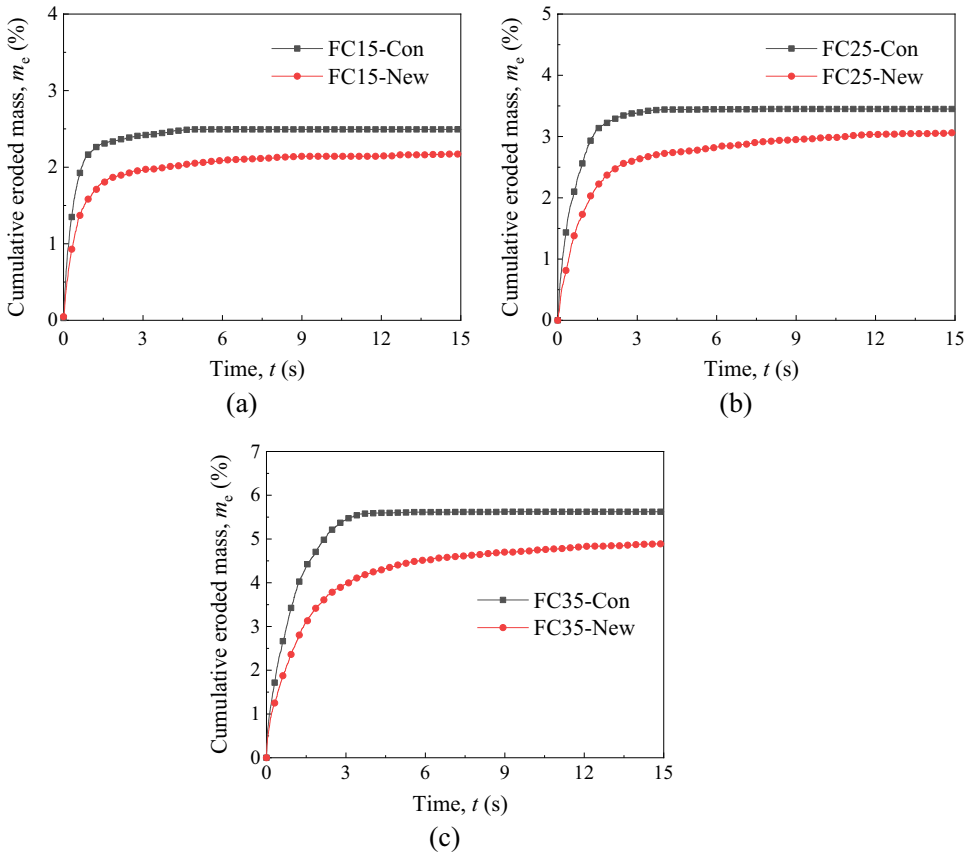

Fig. 5 The cumulative eroded masses vary with the testing time using the conventional and new modeling methods: **a** FC = 15%; **b** FC = 25%; **c** FC = 35%

than FC15-New. Similarly, in the case of FC25-Con, it is 15% higher than FC25-New, and in the case of FC35-Con, it is 14% higher than FC35-New. The primary reason for this difference is that the numerical models generated using the conventional modeling method exhibit higher porosity at the wall boundary, resulting in higher flow velocities. Consequently, this leads to a greater loss of fine particles at the boundaries of the sample. Subsequent sections will provide a more detailed analysis of the sources of eroded fine particles and the flow field in the CFD domain, further elucidating this phenomenon.

Figure 6 shows the distribution of the original position of eroded fine particles in the x–y plane. The conventional method predicts a highly non-uniform distribution and more particle loss occurs at the boundary. The particle loss in the new methods looks quite uniform. When comparing FC15-Con with FC35-Con, the difference in fine particle loss between the boundary and center cells in the case of FC15-Con may appear less significant. This observation is primarily attributed to the relatively lower fines content in the sample, resulting in a smaller discrepancy in the number of particles between the boundary and center cells. To provide a more precise analysis of the difference between the boundary and center cells for all samples, a one-way analysis of variance (ANOVA) was carried out to analyze these observations quantitatively. The statistical analysis was performed using the Statistical Product Service Solutions (SPSS) version 26 (IBM

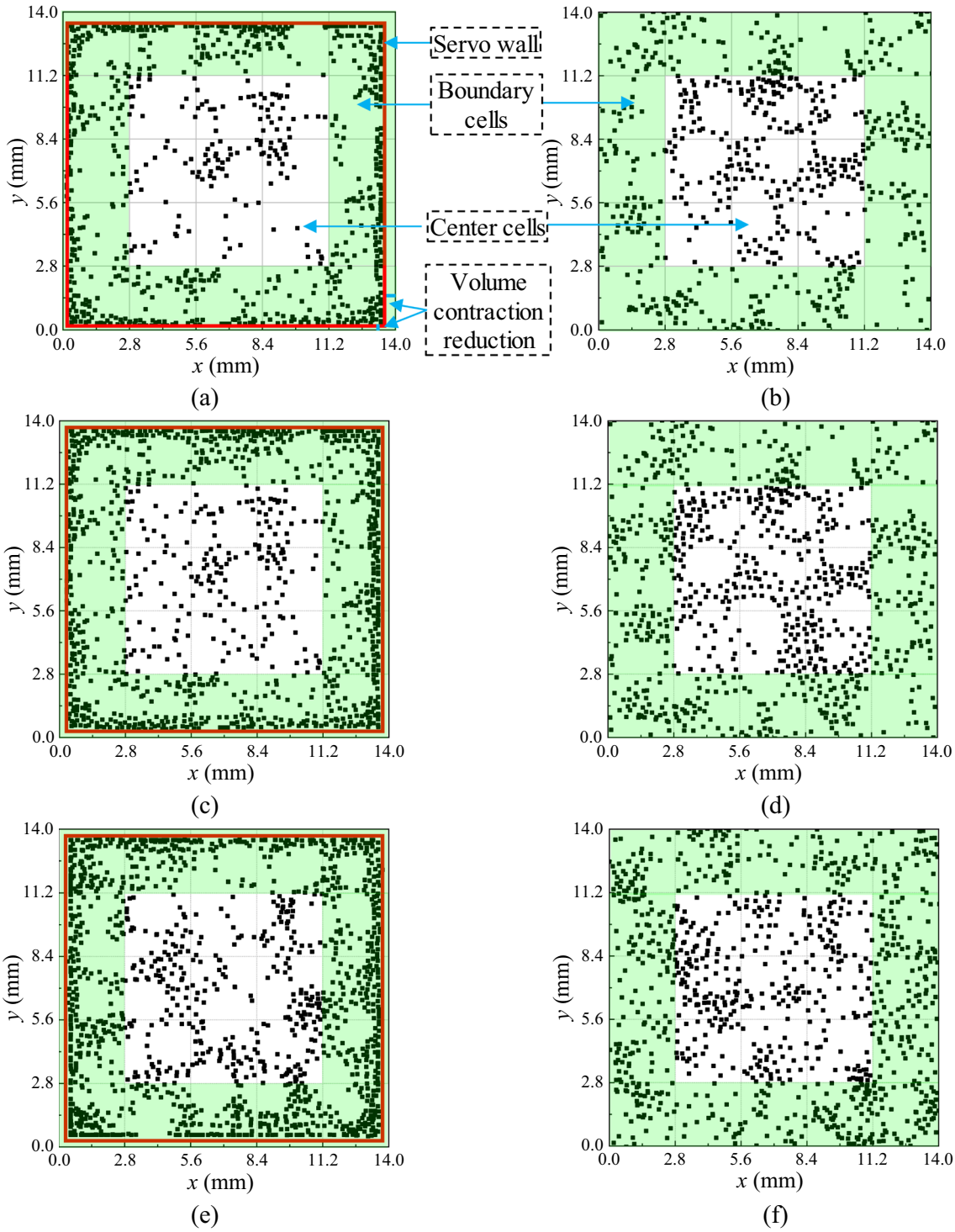

Fig. 6 Distribution of the original position of eroded particles: **a** FC15-Con; **b** FC15-New; **c** FC25-Con; **d** FC25-New; **e** FC35-Con; **f** FC35-New

2012) in terms of 95% confidence level. The results of ANOVA are given in Table 3. In the conventional method, the difference in fine particle loss between the boundary and center cells is significant (i.e., P value < 0.05). In contrast, the difference is not significant in the new method.

Table 3 Comparison of fine particle loss from the boundary and center cells

Sample ID	Source	d.f	Sum of squares	Mean squares	*F*	*P*
FC15-Con	Treatment	1	1.33	1.33	6.24	< 0.001
	Residual	23	0.85	0.04		
	Total	24	2.18			
FC15-New	Treatment	1	0.21	0.21	3.68	N.S
	Residual	23	1.29	0.06		
	Total	24	1.50			
FC25-Con	Treatment	1	1.88	1.88	6.95	0.0179
	Residual	23	1.12	0.26		
	Total	24	2.30			
FC25-New	Treatment	1	0.53	0.53	2.84	N.S
	Residual	23	1.98	0.18		
	Total	24	1.54			
FC35-Con	Treatment	1	0.58	0.58	5.79	0.0104
	Residual	23	1.71	0.07		
	Total	24	2.29			
FC35-New	Treatment	1	0.17	0.17	3.06	N.S
	Residual	23	1.28	0.06		
	Total	24	1.46			

d.f.: degree of freedom; N.S.: not significant

Comparison of velocity distribution

To explain the above results about particle loss, the velocity distributions of the flow field are determined for analysis. In the cases of FC15-Con, FC25-Con, and FC35-Con (see Figs. 7a, 8a, and 9a), the fluid velocity at the boundary is significantly higher than that in the center before erosion (i.e., $t = 0.001$ s). The difference becomes more significant after erosion (i.e., $t = 15$ s), implying that the high fluid velocity along the model walls has eroded more fine particles.

On the contrary, for the cases of FC15-New, FC25-New, and FC35-New, the velocity distributions are much more uniform at the beginning of the erosion tests (see Figs. 7b, 8b, and 9b). It implies that the soil structure modeled by the new method is relatively homogeneous. Moreover, when the erosion tests end (i.e., $t = 15$ s), the velocity distributions remain uniform, indicating no obvious preferential flow occurs in new models.

Comparison between computed and experimental results

Figure 10 shows the comparison between the experimental results (Ke and Takahashi 2014) and computed results. Because the time scales of the experiment and simulation are different, the normalization method is applied (Jäger et al. 2018; Yin et al. 2021). Specifically, in each tested method, the dimensionless time $t_d = t/t_{\text{total}}$, where t is the elapsed time and t_{total} is the total erosion time; the dimensionless eroded mass $m_{\text{ed}} = m_e/m_{e,\ \text{FC=35\%}}$, where $m_{e,\ \text{FC=35\%}}$ is the cumulative eroded mass of sample with FC = 35%. The erosion curves generated by the new method closely align with the experimental results. The difference between the computed results in the new method and the experimental results, particularly during the early testing age (from dimensionless time 0 to 0.4), may be primarily attributed to the shape of soil particles and the method of applying the hydraulic gradient. In contrast, the erosion rate in the conventional method is significantly higher, especially in the early testing age. As a result, it can be concluded that the new method is more suitable for simulating the erosion behavior of soil samples.

Discussion

As mentioned earlier, apparent sidewall preferential flow has been observed in internal erosion simulations on soil samples with different fines contents using the conventional modeling method. It is worth noting that as the fines content increases from 15 to 35%, the difference in cumulative eroded fines mass between the new and conventional methods gradually decreases, reducing from 17 to 14%. The primary reason is that, in simulations with soil samples featuring higher fines content using the conventional method, more fine particles densely fill the wall boundaries, resulting in a more uniform distribution of particles throughout the sample. This leads to a smaller difference in porosity between the wall boundary and the center of the sample, ultimately reducing the sidewall preferential flow effect. This phenomenon is further supported by observations in Figs. 7, 8, and 9. These

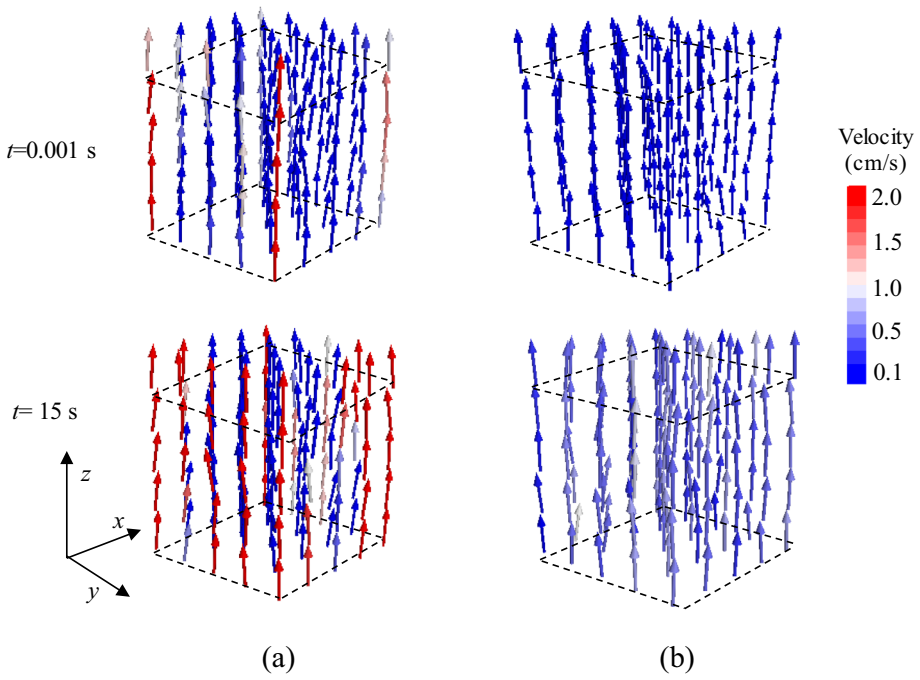

Fig. 7 Fluid velocity distribution computed using the conventional and new methods: **a** FC15-Con; **b** FC15-New

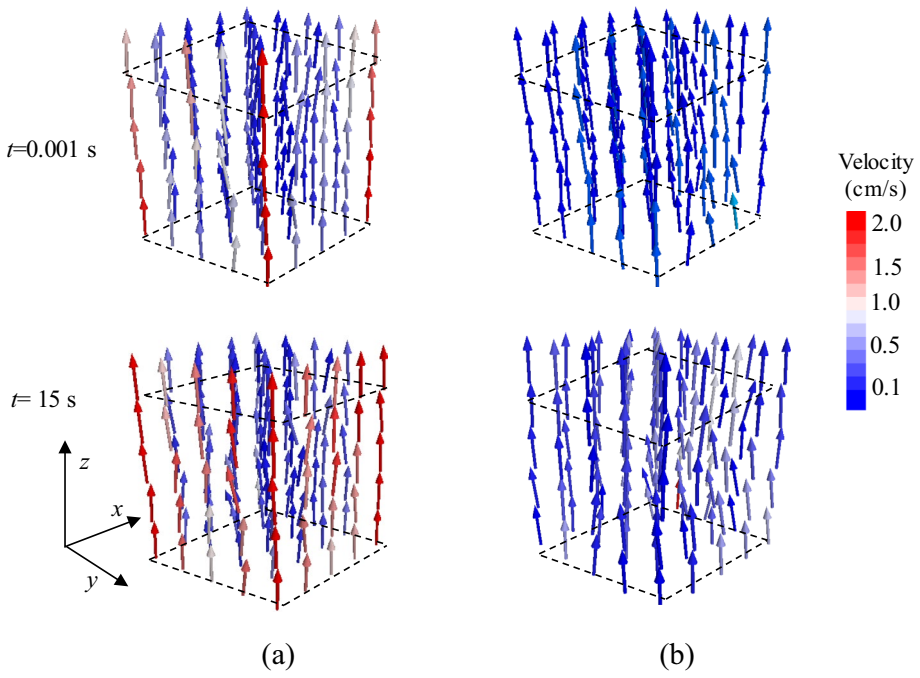

Fig. 8 Fluid velocity distribution computed using the conventional and new methods: **a** FC25-Con; **b** FC25-New

figures reveal that with an increase in fines content, the velocity difference between the sample's wall boundary and center gradually decreases, indicating a diminishing sidewall preferential flow effect.

This observation offers valuable insights and practical implications. Increasing the fine particle content within the soil, particularly near rigid sidewalls, can be an effective means of mitigating sidewall preferential flow. Additionally, for laboratory erosion experiments, the application of binding materials at the wall boundaries can immobilize the particles and replicate the functionality of particle boundaries. It is evident that incorporating particle boundaries into internal erosion simulations is an effective approach for preventing sidewall preferential flow. However, it is important to note that the particle boundary can lead to the generation of more particles, potentially impacting numerical computational efficiency. Therefore, it is necessary to conduct a thorough evaluation of this trade-off and explore potential

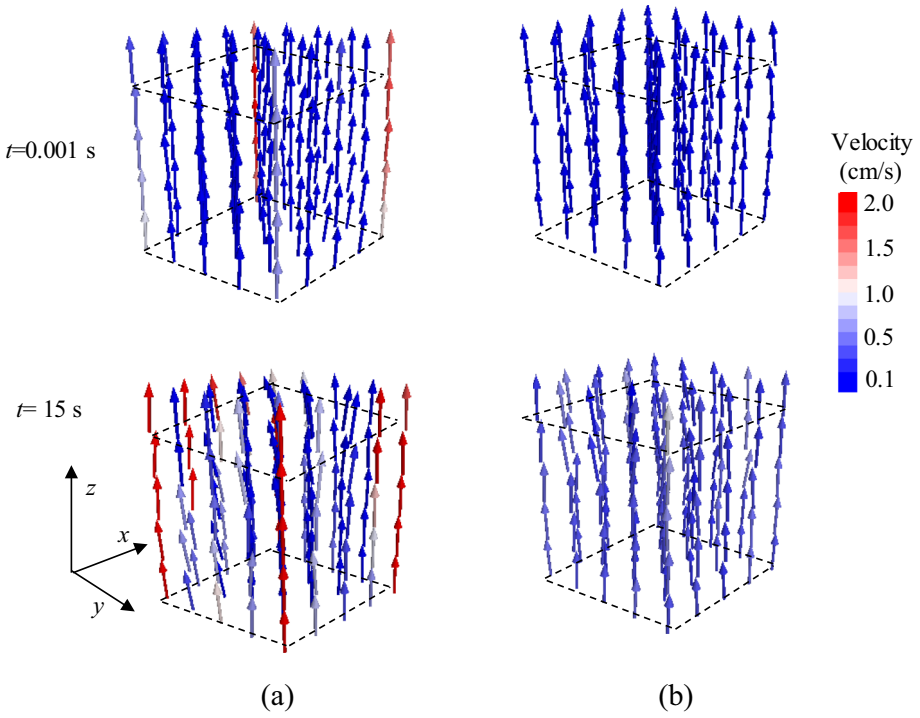

Fig. 9 Fluid velocity distribution computed using the conventional and new methods: **a** FC35-Con; **b** FC35-New

optimizations of particle boundary thickness to enhance computational efficiency in future studies.

One might wonder if this new model can simulate soils containing very fine particles, such as biochar or ash (Chen et al. 2023; Wani et al. 2022), or replicate real field conditions. In theory, simulating these scenarios is indeed possible. However, it is essential to acknowledge that simulating soils with an abundance of such fine particles can significantly impact computational efficiency. Given current computational capabilities, it is not advisable to simulate the soils containing biochar or ash and the real field conditions due to the substantial increase in the number of particles. Instead, it is recommended to use representative volume elements (RVE) to simulate real soil samples.

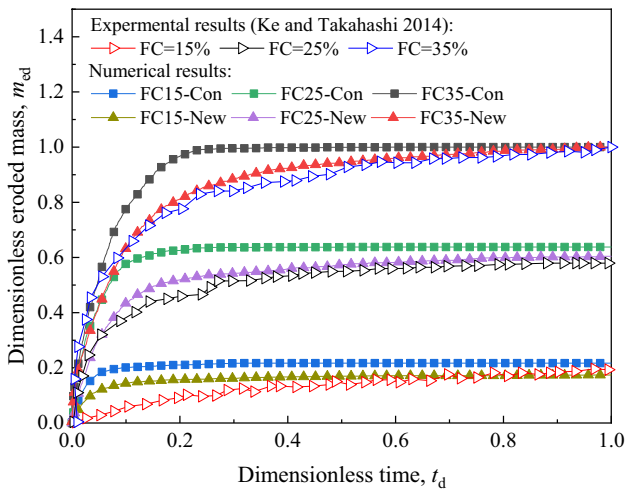

Fig. 10 Numerical results compared with experimental results

Conclusion

Sidewall preferential flow is generally observed in conventional CFD–DEM simulations of internal erosion due to rigid wall boundary conditions and the volume contraction induced by consolidation and seepage erosion. This study proposes a particle boundary instead of a wall boundary to address this problem. The optimal dimensions of the new model under non-displacement boundary and constant-stress boundary conditions have been established. Comparisons of fines loss and velocity distribution in three pairs of numerical tests are conducted, showing that the percentage of cumulative eroded fine particles in the new model is approximately 15% lower than in the conventional model. The new method is verified using experimental results with different fines contents. It suggests that the newly proposed modeling method can simulate internal erosion well and give a more accurate assessment of geomaterial erodibility.

Acknowledgements This work was supported by the National Natural Science Foundation of China through the research grants 52278339, 52022004 and 52209126; The authors also would like to thank the Science and Technology Program of Shenzhen through the grant KQTD20210811090112003.

Funding Open access funding provided by The Hong Kong Polytechnic University.

Declarations

Conflict of interest The authors declare that there is no conflict of interest regarding the publication of this paper.

References

Bendahmane F, Marot D, Alexis A (2008) Experimental parametric study of suffusion and backward erosion. J Geotech Geoenviron Eng 134(1):57–67

Bora MJ, Bordoloi S, Pekkat S, Garg A, Sekharan S, Rakesh RR (2022) Assessment of soil erosion models for predicting soil loss in cracked vegetated compacted surface layer. Acta Geophys 70(1):333–347

Bora MJ, Cai W, Pekkat S, Garg A, Sekharan S (2023) Development of a simplified theoretical model to determine erodibility of compacted soil in hole erosion test based on fluid energy transformation. Acta Geotech 18:5441–5455

Cai W, Bora MJ, Pekkat S, Bordoloi S, Garg A, Sekharan S (2023) A new and simple model for predicting soil erosion based on hole erosion tests. Acta Geophys 71(2):823–836

Chen R, Liu L, Li Z, Deng G, Zhang Y, Zhang Y (2021) A novel vertical stress-controlled apparatus for studying suffusion along horizontal seepage through soils. Acta Geotech 16(7):2217–2230

Chen B, Cai W, Garg A (2023) Relationship between bioelectricity and soil–water characteristics of biochar-aided plant microbial fuel cell. Acta Geotech 18:3529–3542

Cheng K, Zhang C, Peng K, Liu H, Ahmad M (2021) Un-resolved CFD–DEM method: an insight into its limitations in the modeling of suffusion in gap-graded soils. Powder Technol 381:520–538

Cheung G, O'Sullivan C (2008) Effective simulation of flexible lateral boundaries in two- and three-dimensional dem simulations. Particuology 6(6):483–500

Cundall PA, Strack ODL (1979) A discrete numerical model for granular assemblies. Geotechnique 30(3):331–336

Di Felice R (1994) The voidage function for fluid-particle interaction systems. Int J Multiph Flow 20(1):153–159

Garg A, Wani I, Kushvaha V (2022) Application of artificial intelligence for predicting erosion of biochar amended soils. Sustainability 14(2):684

Gu DM, Huang D, Liu HL, Zhang WG, Gao XC (2019) A dem-based approach for modeling the evolution process of seepage-induced erosion in clayey sand. Acta Geotech 14(6):1629–1641

Hu Z, Zhang Y, Yang Z (2019) Suffusion-induced deformation and microstructural change of granular soils: a coupled CFD–DEM study. Acta Geotech 14(3):795–814

Hu Z, Yang ZX, Zhang YD (2020) CFD–DEM modeling of suffusion effect on undrained behavior of internally unstable soils. Comput Geotech 126:103692

IBM (2012) IBM SPSS statistics 21.0. SPSS Inc., Chicago, IL, USA

ICOLD (2013) Internal erosion of existing dams, levees and dikes, and their foundations (ICOLD Bulletin 164), Paris

Itasca Consulting Group A (2015) PFC3D 5.0 User Manual, Minneapolis

Jäger R, Mendoza M, Herrmann HJ (2018) Clogging at pore scale and pressure-induced erosion. Phys Rev Fluids 3(7):74302

Ke L, Takahashi A (2014) Experimental investigations on suffusion characteristics and its mechanical consequences on saturated cohesionless soil. Soils Found 54(4):713–730

Kézdi, (1979) Soil physics: selected topics. Elsevier, Amsterdam

Kim H, Park J, Shin J (2019) Flow behavior and piping potential at the soil-structure interface. Geotechnique 69(1):79–84

Li X, Li X (2023) A soil freezing-thawing model based on thermodynamics. Cold Reg Sci Technol 211:103867

Li Z, Wang YH, Ma CH, Mok CMB (2017) Experimental characterization and 3d DEM simulation of bond breakages in artificially cemented sands with different bond strengths when subjected to triaxial shearing. Acta Geotech 12(5):987–1002

Li G, Zhan TL, Zhang Z, Zhang S, Feng S (2023) Pore network modeling of capillary barrier effects: impact of pore sizes. Can Geotech J 61:174–182

Liu Y, Wang L, Hong Y, Zhao J, Yin Z (2020) A coupled CFD–DEM investigation of suffusion of gap graded soil: coupling effect of confining pressure and fines content. Int J Numer Anal Methods Geomech 44(18):2473–2500

Liu L, Chen R, Zhou C, Li X, Bate B (2023) Microscopic mechanism of the combined effects of confining pressure and fines content on suffusion in gap-graded underfilled soils. J Hydrol 626:130370

Mu L, Zhang P, Shi Z, Huang M (2022) Coupled CFD–DEM investigation of erosion accompanied by clogging mechanism under different hydraulic gradients. Comput Geotech 153:105058

Nguyen TT, Indraratna B (2020) A coupled CFD–DEM approach to examine the hydraulic critical state of soil under increasing hydraulic gradient. Int J Geomech 20(9):4020131–4020138

Nie Y, Lan L, Yan X, Wang X (2023) Effect of gradation variation on particle transport process in a generalized flash flood gully via CFD–DEM method. Acta Geophys 71(1):391–404

Nijssen TMJ, Ottens M, Padding JT (2023) A note on the modeling of lubrication forces in unresolved simulations. Powder Technol 413:118017

Premkumar S, Piratheepan J, Arulrajah A, Disfani MM, Rajeev P (2016) Experimental study on contact erosion failure in pavement embankment with dispersive clay. J Mater Civ Eng 28(4):04015179

Shi ZM, Zheng HC, Yu SB, Peng M, Jiang T (2018) Application of CFD–DEM to investigate seepage characteristics of landslide dam materials. Comput Geotech 101:23–33

Wang X, Huang B, Tang Y, Hu T, Ling D (2022) Microscopic mechanism and analytical modeling of seepage-induced erosion in bimodal soils. Comput Geotech 141:104527

Wani I, Kushvaha V, Garg A, Kumar R, Naik S, Sharma P (2022) Review on effect of biochar on soil strength: toward exploring usage of biochar in geo-engineering infrastructure. In: Biomass conversion and biorefinery, pp 1–32

Xiong H, Yin Z, Zhao J, Yang Y (2021) Investigating the effect of flow direction on suffusion and its impacts on gap-graded granular soils. Acta Geotech 16(2):399–419

Yao LM, Xiao ZM, Liu JB, Zhang Q, Wang M (2020) An optimized CFD–DEM method for fluid-particle coupling dynamics analysis. Int J Mech Sci 174:105503

Yin Y, Cui Y, Tang Y, Liu D, Lei M, Chan D (2021) Solid–fluid sequentially coupled simulation of internal erosion of soils due to seepage. Granul Matter 23(2):20

Zhang P, Mu L, Huang M (2023) A coupled CFD-DEM investigation into hydro-mechanical behavior of gap-graded soilexperiencing seepage erosion considering cyclic hydraulic loading. J Hydrol 624:129908

Zhao J, Shan T (2013) Coupled CFD–DEM simulation of fluid-particle interaction in geomechanics. Powder Technol 239:248–258

Zhou ZQ, Ranjith PG, Li SC (2018) An experimental testing apparatus for study of suffusion of granular soils in geological structures. Tunn Undergr Space Technol 78:222–230

Zou Y, Chen C, Zhang L (2020) Simulating progression of internal erosion in gap-graded sandy gravels using coupled CFD–DEM. Int J Geomech 20(1):4019135